Eur. Phys. J. Special Topics **213**, 343–353 (2012)

DOI: 10.1140/epjst/e2012-01681-4

THE EUROPEAN PHYSICAL JOURNAL SPECIAL TOPICS

Regular Article

Protein adsorption properties of OEG monolayers and dense PNIPAM brushes probed by neutron reflectivity

N. Brouette[1], C. Xue[2], M. Haertlein[3], M. Moulin[3], G. Fragneto[3], D.E. Leckband[2,4], A. Halperin[5], and M. Sferrazza[1,a]

[1] Département de Physique, Faculté des Sciences, Université Libre de Bruxelles, Boulevard du Triomphe, CP. 223, 1050 Bruxelles, Belgique
[2] Department of Chemical and Biomolecular Engineering, University of Illinois at Urbana-Champaign, Urbana, Illinois 61801, USA
[3] Institut Max Von Laue-Paul Langevin, 38042 Grenoble, France
[4] Department of Chemistry, University of Illinois at Urbana-Champaign, Urbana, Illinois 61801, USA
[5] University of Grenoble 1/CNRS, LIPhy UMR 5588, BP. 87, 38041 Grenoble, France

Received 20 July 2012 / Received in final form 27 September 2012
Published online 3 December 2012

Abstract. The structure of dense poly(N-isopropylacrylamide) (PNIPAM) brushes and oligo(ethylene glycol) (OEG) monolayers has been probed using neutron reflectometry and ellipsometry. The PNIPAM brush is swollen below the Lower Critical Solution Temperature (LCST) of 32 °C and is collapsed at 37 °C. Neutron reflectivity shows that below the LCST, the brush is described by a two-layer model: an inner dense layer and a hydrated outer layer. Above the LCST the collapsed brush forms a homogenous layer. With a fully deuterated myoglobin protein to increase the neutron scattering length density contrast, the reflectivity data show no detectable primary adsorption on the grafted OEG surface. A bound on the ternary adsorption onto PNIPAM chains forming dense brushes below and above the LCST is obtained.

1 Introduction

Understanding protein adsorption on solid surfaces in aqueous environments is a crucial step for both fundamental and applied point of views, including, for example, the identification of interactions mediating the adsorption process, the use of proteins for colloidal stabilization, the development of surgical implants, or the development of biosensors. In particular, protein adsorption is responsible for a variety of technologically undesirable processes, such as contact lenses fouling, clotting on blood-contacting devices, triggering inflammation around artificial organs, or reducing the circulation time of therapeutic proteins and drug bearing liposomes [1].

[a] e-mail: msferraz@ulb.ac.be

The development of antifouling surfaces represents, in general, a technical challenge. Recently, some studies [2–4] have shown that surfaces modified with Polyethylene Oxyde (PEO) or with poly(*N*-isopropylacrylamide) (PNIPAM) can, in certain regimes, decrease considerably the protein adsorption. Surfaces coated with PEO brushes are known to reduce the amount of absorbed protein depending on the grafting density and also on the bulk protein concentration [5–7]. However, in all case, the adsorbed amount is no negligible and the adsorbed amount is more important for higher bulk protein concentration. Moreover, no study has shown that PEO brushes are totally antifouling. Two main types of adsorption modes are generally assumed for small globular protein onto polymer brushes: "primary" adsorption at the grafting surface and "ternary" adsorption within the brush due to polymer-protein attraction [8,9]. "Secondary" adsorption at the outer edge of the brush can also occur, but only for large proteins [10].

PNIPAM is a thermosensitive polymer that undergoes a reversible collapse above the lower critical solution temperature (LCST) of 32 °C. Below the LCST, the polymer is swollen in water, but dense PNIPAM chains generally collapse above the LCST [11,12]. Recently, Xue et al. demonstrated by ellipsometry, radio assay, and fluorescence imaging that dense PNIPAM brushes prepared using the "grafting from" method by surface-initiated atom transfer radical polymerization (ATRP), admit very low level of adsorbed protein [11]. In particular, it was shown by radio assay that, PNIPAM brushes admit about 0.2 mg/m^2 of adsorbed protein below the LCST. Above the LCST, the adsorbed amount was between 0.3 mg/m^2 and 0.6 mg/m^2 depending on the grafting density [11]. In another example, cell attachment on PNIPAM hydrogels polymerized by electron beam irradiation on tissue culture polystyrene or on glass depends on the gel thickness, with the thicker gels repelling cells above and below the LCST [13–15](cell adhesion requires previously adsorbed protein). In the latter example, fibronectin adsorbed on thin (15–20 nm) PNIPAM gels but not on thick (>30 nm) coatings [14,15]. Plasma-deposited PNIPAM coatings reversibly adsorb protein above the 32 °C, regardless of the film thickness [16].

Therefore, the antifouling properties appear to strongly depend on the properties and synthesis of the PNIPAM coating.

In this study, we investigated protein adsorption on surfaces modified with an oligo(ethylene glycol) (OEG) monolayer at 25 °C and with dense and lengthy PNIPAM brushes, both at 25 °C and at 37 °C, using neutron reflectivity and ellipsometry. The PNIPAM brushes were prepared using the "grafting from" method by surface-initiated atom transfer radical polymerization (ATRP). Neutron Reflectometry (NR) enables determination of the volume fraction profile of the PNIPAM both below and above the LCST. We have studied the adsorption of the globular deuterated myoglobin, in order to test protein adsorption on OEG and PNIPAM.

2 Materials and methods

2.1 Chemicals

N-isopropylacrylamide (NIPAM), and 1,1,4,7,7-penta-methyldiethylenetriamine (PMDETA) were purchased from Acros. NIPAM monomer was re-crystallized from hexane. 2-[methoxy(polyethyleneoxy)propyl]-trimethoxysilane (OEG) was from Gelest Inc. CuBr, methanol and anhydrous toluene were purchased from Aldrich. The initiator, 11-(2-Bromo-2-methyl)-propionyloxy undecyl trichlorosilane, was synthesized as described [17]. All aqueous solutions were prepared with Milli-Q purified water (Millipore, Bedford, MA) with a resistivity of 18.2 MΩ • cm. D_2O(> 99%) was provided by the ILL.

2.2 Deuterated myoglobin solution

The protein used is a 100% deuterated myoglobin of 20.6 kDa and has a scattering length density (SLD) of 6.75×10^{-6} Å^{-2} in H_2O. It is a roughly spherical protein with a diameter of 39 Å [18]. The protein was deuterated and purified at the ILL Deuteration Laboratory using the procedure described in [19]. The myoglobin solution was prepared in a 20 mM Tris and 50 mM NaCl Buffer at pH 7.5. The isoelectric point of myoglobin is 7.2 [18]. So at pH 7.5, the protein can be considered as globally neutral.

2.3 Grafting of OEG monolayer

Firstly, the silicon wafer was cleaned using the "piranha solution" ($1:3\ H_20_2 : H_2SO_4$) for a few minutes and was thoroughly rinsed afterwards with ion exchanged water. Self-assembled monolayers of OEG were formed on the substrates by immersing the clean silicon wafers in a toluene solution containing 2 mM of OEG for 4 Hours [20]. The grafting reaction is very sensitive to the amount of water in the environment [21]. So, we used anhydrous toluene and the reaction is performed on a dessicator to minimize the uptake of water. Then, the samples were rinsed with toluene to remove the excess of OEG.

2.4 Surface-Initiated polymerization of the N-Isopropylacrylamide brush

The poly(N-isopropylacrylamide) (PNIPAM) brush was synthesized by surface initiated atom transfer radical polymerization (ATRP) of N-isopropylacrylamide from initiator functionalized silicon substrates according to published procedure [12]. First, self-assembled monolayers of the initiator (SAM-Br) were formed on the substrates by immersing the clean silicon wafers in a toluene solution containing 2 mM of the initiator silane for 4 hr. The substrates were then placed in a reaction vessel and degassed with three freeze-pump-thaw cycles. NIPAM (3.955 g, 35 mmol) was dissolved in a mixture of $MeOH/H_2O$ (v/v : 7/3) and degassed with nitrogen for 1 hour [21]. The catalyst, CuBr (50.75 mg, 0.35 mmol), and the ligand, PMDETA (227.92 μL, 1.05 mmol), were then added to the monomer solution. This mixture was transferred, via a cannula, into the reaction vessel containing the silicon wafers functionalized with only $SAM - Br$ (100% initiator). The polymerization reaction was at room temperature under a nitrogen atmosphere, for 1 hour. At the end of the reaction, the vessels were disconnected from the nitrogen line and the substrates were rinsed extensively with methanol, followed by sonication in methanol, ethanol, and then water before drying under a stream of nitrogen. The surface coverage σ was estimated from the maximum packing density of 2.1 bromine initiator/nm^2 [11].

2.5 Neutron reflectivity

The NR measurements were performed in the Institut Laue-Langevin (ILL, Grenoble, France) using the D17 reflectometer. In a neutron reflectivity experiment, we measure the specular reflection as a function of the transfer wave vector q perpendicular to the surface – $q = \frac{4\pi}{\lambda} \sin\theta$ where θ is the incident angle and λ is the wavelength. The wavelengths of the incident neutrons are between about 2 Å and 20 Å [22]. We used the time-of-flight configuration and the NR profiles were recorded at two fixed incident angles in order to cover the desired q range. The measurement cell consisted of a PTFE (poly(tetrafluoroethylene)) reservoir containing the water solutions put against the

silicon block sandwiched between two aluminium plates. Single-crystalline and (111) polished silicon substrates ($5 \times 5 \times 1\,\mathrm{cm}^3$) were used (Siltronix, France). The neutron reflection experimental profiles were fitted by a box model. We used the contrast variation method consisting of using water of different scattering length densities by mixing H_2O and D_2O, allowing us to enhance sensitivity of certain components of the system. The contrasts used were D_2O, 4MW, and H_2O. 4MW is a contrast liquid that has a scattering length density of $4 \times 10^{-6}\,\text{Å}^{-2}$. So, the SLD are $6.35 \times 10^{-6}\,\text{Å}^{-2}$, $4 \times 10^{-6}\,\text{Å}^{-2}$ and $-0.56 \times 10^{-6}\,\text{Å}^{-2}$, respectively for D_2O, 4MW and H_2O.

2.6 Ellipsometry

Ellipsometry was used to determine the thickness and the refractive index of the thin films by measuring the change in the polarization of an incident light after reflection on a flat surface. Ellipsometry measures the ellipticity ρ : $\rho = \tan\Psi e^{j\Delta}$ where $\tan\Psi$ is the ratio of light amplitudes before and after reflection and Δ is the phase difference introduced by reflection. The measured data are modelled by a box model. We used a Horiba Jobin–Yvon MM-16 spectroscopic phase modulated ellipsometer. The light source is a halogen and a LED lamp (430 nm to 850 nm). All the measurements were performed near the Brewster angle at an incidence of 70° and utilize the entire spectral range. The measurements at the solid/liquid interface were carried out in a homemade cell which is temperature regulated by a water bath.

3 Results and discussion

The dry thickness of the OEG monolayer measured by ellipsometry is (13 ± 3)Å (the silicon oxide layer was previously characterized to be (17 ± 2)Å). These values are in good agreement with other studies [20,23]. Considering this thickness, an OEG density of $1.13\,\mathrm{g/cm}^3$ and an average molecular weight of $538\,\mathrm{g/mol}$, we calculate a surface excess of about $0.15\,\mu\mathrm{g/cm}^2 (2.8\,\mu\mathrm{Mol/m}^2)$. The determined wet thickness in the Tris buffer is (23 ± 5)Å. During the fits, the thickness of the oxide layer was kept constant at 17 Å. From the fit of the refractive index, we also deduce that the OEG monolayer contains $(47 \pm 7)\%$ water. The thickness and the refractive index determined by ellipsometry of the dry and wet OEG monolayer are summarized in Table 1 where the percentage of solvent is also given for the wet OEG. The OEG monolayer has been also characterized with NR in two different contrast liquids, H_2O and D_2O and the reflectivity profiles as a function of momentum transfer q of the OEG system in the two contrasts are shown in Fig. 1.

The system was modeled using a series of slabs. The SLDs are fixed at $2.07 \times 10^{-6}\,\text{Å}^{-2}$for silicon, $3.4 \times 10^{-6}\,\text{Å}^{-2}$ for silicon oxide and $0.44 \times 10^{-6}\,\text{Å}^{-2}$ for OEG. The lines in Fig. 1 are the fits obtained. The silicon oxide layer is found to be (15 ± 2)Å thick and it contains $(12 \pm 4)\%$ of water. The water in the oxide layer is probably due to pre-treatment of the wafer by "piranha solution" which makes the oxide layer porous [24]. The values obtained are in good agreement with other reports [25–27]. The OEG thickness is found to be (19 ± 2)Å and containing $(63 \pm 5)\%$ of solvent. These values agree with the wet thickness that we found by ellipsometry (Table 1).

The dry thickness of the PNIPAM brush has been characterized by ellipsometry and by NR. A thickness of (899 ± 9)Å (Table 1) is obtained with ellipsometry whereas we obtained a thickness layer of (896 ± 8)Å with a roughness of (17 ± 11)Å by NR. The dry thickness allows us to estimated the number average molecular weight M_N of the grafted PNIPAM using equation $M_N = \dfrac{h\rho N_A}{\sigma}$, where h is the measured brush

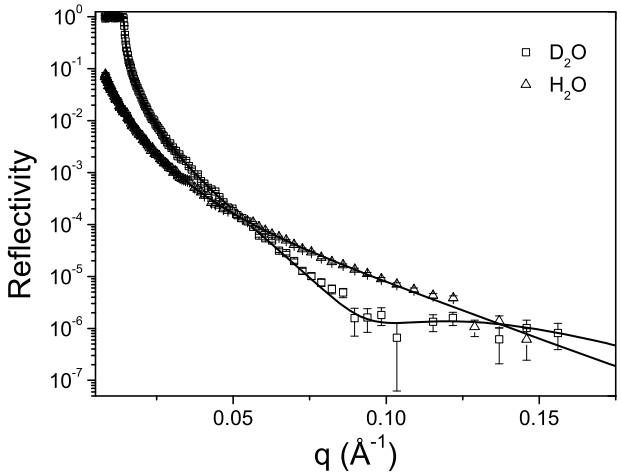

Fig. 1. Reflectivity profiles of the OEG self assembled monolayer in two contrasts: D_2O (square) and H_2O (triangle). The lines are the fit of the data.

Table 1. Thickness, Refractive Index at 546 nm and % solvent determined by ellipsometry for OEG (dry and wet) and for PNIPAM (dry, wet at 25 °C and wet at 37 °C).

	Thick (Å)	n at 546 nm	% solv (%)
Dry OEG	13 ± 3	1.479 ± 0.005	/
Wet OEG	23 ± 5	1.41 ± 0.005	47 ± 7
Dry PNIPAM	899 ± 9	1.494 ± 0.001	/
Wet PNIPAM at 25 °C	1273 ± 12	1.440 ± 0.001	31 ± 2
Wet PNIPAM at 37 °C	1050 ± 14	1.471 ± 0.001	14 ± 1

thickness, ρ is the density of dry NIPAM (a monomer density of 0.95 g/cm^3 is used [28]), N_A is Avogadro's number and σ is the chain density, which was estimated from the maximum packing density of 2.1 bromine initiator/nm^2 and a chain initiation efficiency of $\sim 10\%$, reported for polystyrene [29,30]. So, the grafting density of the brush is estimated to be 0.21 nm^{-2} and a value of $M_N = 244\,300$ g/mol is then obtained for the molecular weight. To determine whether the polymers are in the brush regime, we calculated the distance between grafting sites – s – relative to the Flory radius $R_F = LN^{3/5}$ [31], assuming that water is a good solvent for PNIPAM. Here L is the monomer size ($\sim$3 Å), and $N = 2162$ is the degree of polymerization. If $s \ll 2R_F$, the chains are in the brush regime [32]. Based on these calculations, we found $R_F = 301$ Å and $s = 22$ Å. Therefore, the chains are thus crowded and form an extended brush.

The PNIPAM brush was also characterized by ellipsometry, in the wet state at 25 °C and at 37 °C, in order to obtain the thickness, the refractive index, and the quantity of solvent within the brush. Both the thickness and the refractive index were obtained from fits, using a Cauchy model. At 25 °C, the determined thickness is (1273 ± 12)Å and the refractive index at 546 nm is 1.44. At 37 °C, the thickness decreased to (1050 ± 14)Å and the refractive index at 546 nm is 1.47. The decrease of the thickness and the increase of the refractive index indicate, as previously suggested, a more non-polar core above the LCST [11,33–36]. So, these data show that the dense PNIPAM brush collapses above the LCST. Two regimes were reported for dense PNIPAM brushes [11,12]: the higher molecular weight chains (>85 kDa) which collapsed above the LCST, and the lower molecular weight chains (<48 kDa) which

Table 2. Fitted parameters (thickness – Thick; % solvent and roughness – Rough) obtained by neutron reflectivity for the dry, swollen and collapsed PNIPAM brush.

	Layer 1			Layer 2		
	Thick (Å)	% Solv (%)	Rough (Å)	Thick (Å)	% Solv (%)	Rough (Å)
Dry PNIPAM	896 ± 8	/	17 ± 11	/	/	/
Wet PNIPAM (25 °C)	1022 ± 52	32 ± 3	167 ± 82	727 ± 117	76 ± 13	211 ± 31
Wet PNIPAM (37 °C)	1049 ± 8	26 ± 5	45 ± 6	/	/	/

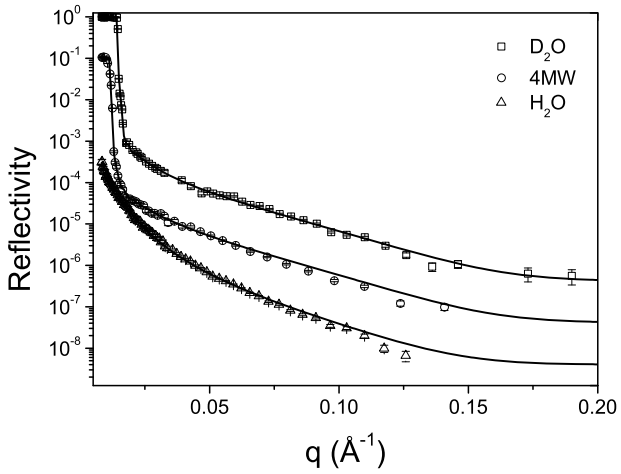

Fig. 2. Reflectivity profiles of the PNIPAM brush at 25 °C (swollen brush) in the three contrasts: D_2O (square), 4MW (circle) and H_2O (triangle). The lines are the fit of the data. For clarity, reflectivity from 4MW is divided by 10 and from H_2O by 100.

remained swollen above 32 °C. These brushes correspond to the former category. The quantity of solvent in the brush was also estimated from the refractive index obtained by the fit and was $(31 \pm 2)\%$ and $(14 \pm 1)\%$ at 25 °C and 37 °C, respectively. These results obtained by ellipsometry are summarized in Table 1. They confirm that at 25 °C, the brush is swollen in water, but that the brush collapses and expels water above the LCST.

The PNIPAM brush was then characterized by NR in order to obtain the volume fraction profile of the brush below and above the LCST. The reflectivity profiles measured as a function of q in D_2O, 4MW and H_2O at 25 °C and 37 °C are shown in Fig. 2 and Fig. 3 respectively. For clarity, the reflectivity profile from 4MW is divided by 10, and the profile from H_2O is divided by 100. The SLD of PNIPAM was calculated to be 0.7×10^{-6} Å^{-2}, by considering a PNIPAM density of 0.95 g/cm^3 [28]. The silicon oxide layer is found to be (22 ± 3)Å thick, and is formed by SiO_2 and $(19 \pm 4)\%$ of water. Those values are in good agreement with previous publications [24–27]. The SAM layer is (24 ± 4)Å thick, and contains $(14 \pm 8)\%$ water. At 25 °C, the brush cannot be modeled by a single layer, but it is described by a two-layer model with a more hydrated layer on the top. At 37 °C, above the LCST, the collapsed brush profile forms a homogeneous layer, within the resolution of these measurements. The fitted parameters for the swollen and collapsed brush are given in Table 2.

Below the LCST, the PNIPAM brush profile has an inner layer of about (1022 ± 52)Å and it contains $(32 \pm 3)\%$ solvent. The outer layer is (727 ± 117)Å thick and contains $(76 \pm 13)\%$ solvent. The total thickness of the swollen brush determined by

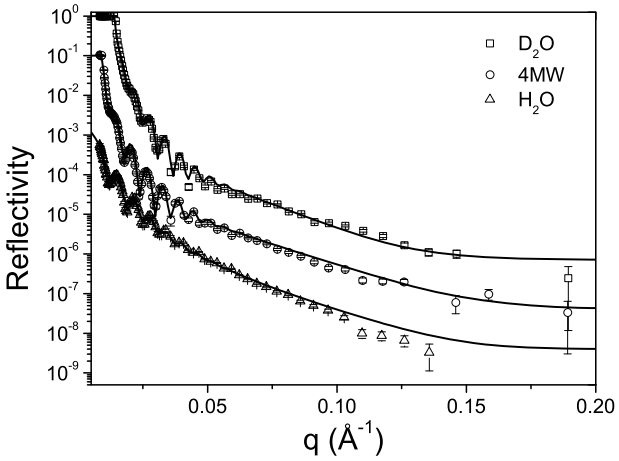

Fig. 3. Reflectivity profiles of the PNIPAM brush at 37 °C (collapsed brush) in the three contrasts: D_2O (square), 4MW (circle) and H_2O (triangle). The lines are the fit of the data. For clarity, reflectivity from 4MW is divided by 10 and from H_2O by 100.

NR is (1749 ± 169)Å, while a value of (1273 ± 12)Å was obtained by ellipsometry. One needs to notice that ellipsometry is less sensitive to the outer layer, which is more hydrated and rougher. However, considering a uniform layer of thickness (1273 ± 12)Å and a water content of (31 ± 2)%, the polymer mass is consistent with the one obtained from NR. NR shows clearly the presence of the two layers within the water-swollen brush.

At 37 °C, above the LCST, the collapsed brush is fitted by a single (1049 ± 8)Å thick layer containing (26 ± 5)% water, in good agreement with the ellipsometry results. Fig. 4a shows scattering length density profile of the PNIPAM brush in 4MW contrast both at 25 °C and at 37 °C, as deduced from the fitting analysis. In Fig. 4b, the volume fraction profile of PNIPAM at 25 °C and at 37 °C shows the existence of superficial swollen chains. The profiles are similar to those obtained by Yim et al [37]. This extension of hydrated chains beyond a dense polymer layer was predicted by theory [38–40]. The polymer-solvent interaction is described by a effective Flory parameter $\chi_{eff}(T, \phi)$, which also depends on the monomer volume fraction ϕ. This dependence influences the swelling and collapse properties, and allows for the possibility of vertical phase separation within the brush. Force measurements also support the existence of superficial swollen chains [12, 41].

The adsorption of proteins on the OEG monolayers was performed using a deuterated myoglobin solution, at a protein concentration of 1 mg/ml. After 8 hours of immersion, the protein solution was removed using the H_2O contrast, and the reflectivity profile was measured.

The NR profiles before and after insertion of the deuterated protein on the OEG surface in H_2O contrast are shown in Fig. 5. For this contrast the sensitivity of the adsorbed amount measurement should be maximal. The profiles did not change after protein immersion, as visible in the Fig. 5, suggesting little or no protein adsorption. To consider the sensitivity of the technique to deuterated protein adsorption, the inset in the Fig. 5 shows simulations of adsorbed proteins modeled by a layer of 40 Å (corresponding to the protein size), where the protein volume fraction in the layer is gradually increased. Protein volume fractions of 2%, 10% and 20% in the adsorbed layer on the top of the OEG are shown in the inset. Clearly the NR profile begin to

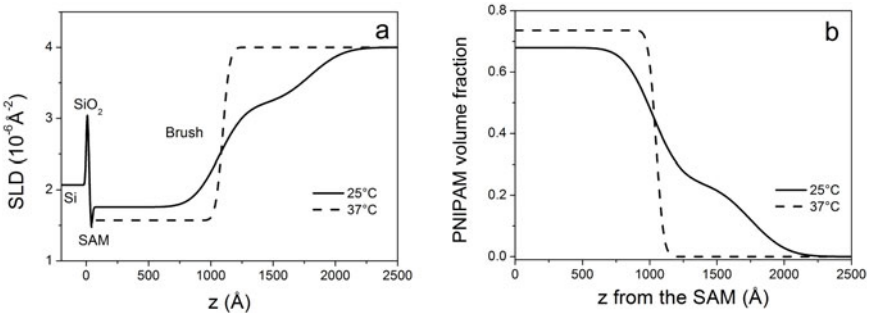

Fig. 4. (a) Scattering length density profile in 4MW contrast at 25 °C (continuous line) and at 37 °C (dashed line); (b) Volume fraction profile of PNIPAM from the SAM at 25 °C (continuous line) and at 37 °C (dashed line).

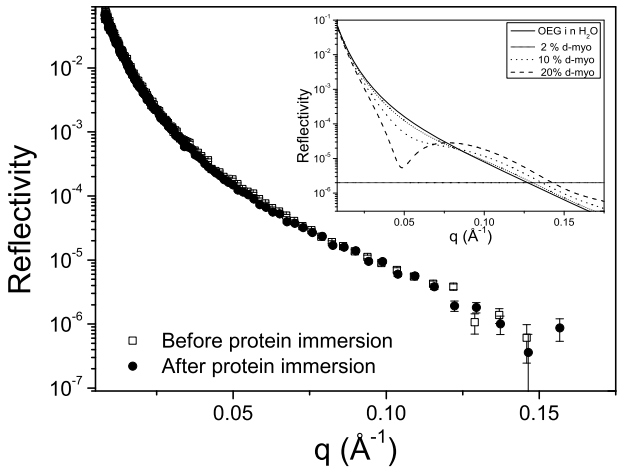

Fig. 5. Reflectivity profiles of OEG monolayer in H_2O before (square) and after (circle) insertion of the deuterated myoglobin solution. Inset: simulation of the change of the reflectivity corresponding to volume fraction of 2%, 10% and 20% of adsorbed deuterated myoglobin on the top of the monolayer (primary adsorption).

differ from the one of the bare OEG interface at protein volume fraction of around 2% corresponding to an adsorbed amount of 0.1 mg/m^2. Since our NR profiles before and after the adsorption overlap, the protein adsorbed amount is below 0.1 mg/m^2. In the inverse system, hydrogenated myoglobin in D_2O, a volume fraction of 2% is not detectable and the lower detectable volume fraction is around 8% indicating that the use of deuterated myoglobin considerably increase the contrast.

Sharma et al. also demonstrated antifouling properties of OEG by using fluorescein isothiocyanate labeled bovine serum albumin [21]. Cecchet et al. similarly showed the protein repellency of OEG by X-ray photoelectron spectroscopy (XPS), using a membrane protein (P.69 antigen)[42].

The NR results indicates that primary adsorption can be repressed by OEG monolayers. Accordingly when such layer is deployed at the grafting surface of the polymer brush, only ternary adsorption should be possible. The reflectivity profiles of PNIPAM brushes before and after the incubation with deuterated proteins were identical, within error bars, for both 25 °C and 37 °C. Figure 6 shows, as an example, the measurement at 37 °C, suggesting again little or no protein adsorption. In this case the

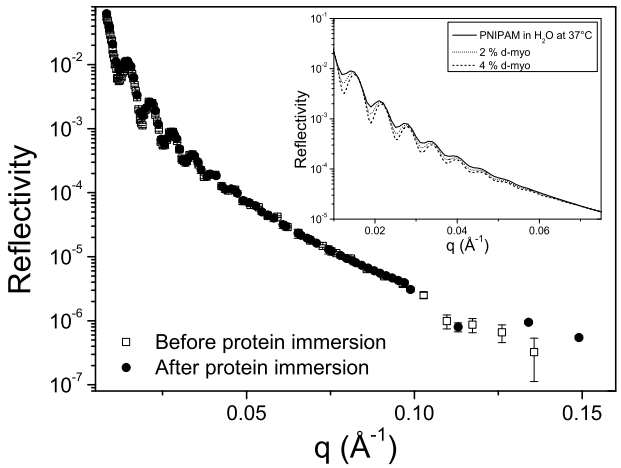

Fig. 6. Reflectivity profiles of the PNIPAM brush at 37 °C in H_2O before (square) and after (circle) insertion of the deuterated myoglobin solution. Inset: simulation of the change of the reflectivity corresponding to volume fraction of 2%, 4% of adsorbed deuterated myoglobin within the brush (ternary adsorption).

thickness of the polymer layer is around 1000 Å, so the sensitivity of the technique to small adsorbed amount is an interesting point since primary adsorption was already excluded by the OEG measurement. The inset in the figure shows a simulation of the change in the NR profile if an uniform ternary adsorption is considered: In this case, volume fractions from 2% upwards are discernible. We need to stress that a difference of 2% relates to a very thick PNIPAM brush of around 1000 Å. Due to this, an adsorbed quantity of about 2 mg/m^2 changes the reflectivity profile. On the other hand, simulations (not shown) with hydrogenated myoglobin show that the minimal detectable volume fractions are around 8% indicating again the advantages of using a deuterated protein. Our work was motivated by the aim of eventuality probing ternary adsorption onto the chains as driven by weak monomer-protein attraction. While Quartz Crystal Microbalance or Surface Plasmon Resonance are sensitive to very small adsorbed amount, they cannot distinguish between primary and ternary adsorption. Thus combining these techniques with NR should yield a full picture of the absorption process.

Since the volume fraction of adsorbed protein is lower than 2% – 3% for this thick brush, these results seem to indicate that dense, high molecular weight PNIPAM brushes are relatively resistant to protein adsorption.

This result could be rationalized considering the structure of the brush. The absence of adsorption within the brush at 25 °C could be related to the presence of the hydrophilic, superficial region, which may present a kinetic barrier to adsorption to the less polar core. For the collapse brushes at 37 °C, surprisingly no adsorption was detected. We may argue that due to the roughness of the layer of around 50 Å, the few first nanometers of the top surface of the collapsed brush remain in average hydrophilic. A tail of the profile going into the water subphase indicates a lower polymer concentration and a higher water content in the first 20 Å. Water contact angle measurements done on this type of dry brushes showed that the contact angle for PNIPAM at 37 °C is around 70 ° while it is around 50 ° for 25 °C indicating the not hydrophobicity of the top surface of the collapsed brush [11]. In the case of thick (>30 nm) PNIPAM gels, Akiyama et al. showed (using a captured air bubble) that

the contact angle of the water swollen brush is little difference above or below the LCST [14]. In addition, protein insertion into dense PNIPAM brushes incurs a high osmotic penalty thus reducing the adsorbed amount [43].

4 Conclusions

OEG monolayer and dense PNIPAM brush were characterized in the dry and wet state by ellipsometry and neutron reflectivity. Neutron reflectivity shows that a dense PNIPAM brush exhibits a two-layer structure below the LCST. The volume fraction profile of the swollen brush at 25 °C, clearly shows that the brush is hydrophilic at the outer edge. Indeed the swollen brush is described by an inner dense layer and an outer, quite hydrated layer. Above the LCST, the PNIPAM is collapsed. The adsorption of deuterated myoglobin on these surfaces was probed: on OEG we did not observe primary adsorption indicating that the surface repels the protein, while on the PNIPAM a bound on the detection sensitivity of ternary adsorption has been extracted. The possibility that the hydrophilic, exterior region, may present a kinetic barrier to adsorption onto the less polar core has been discussed as a possible rationalization of the weak adsorption.

Nicolas Brouette is a PhD student at the Université Libre de Bruxelles, Belgium. He performed the experiments, analyzed the data and contributed to the writing of the paper. Changying Xue and Deborah E. Leckband provided the OEG and PNIPAM system. Michael Haertlein and Martine Moulin deuterated the protein. The authors thank ILL for providing the beam-time. The project is a collaboration among Deborah E. Leckband, Giovanna Fragneto, Avraham Halperin and Michele Sferrazza. Financial support for the project was provided by FNRS of Belgique.

References

1. J.M. Harris, *Poly(Ethylene Glycol) Chemistry: Biotechnical and Biomedical Applications* (Plenum Press, New York, 1992)
2. M. Malmsten, *Biopolymers at Interfaces* (M. Dekker, New York, 2003)
3. J. Goddard, J. Hotchkiss, Prog. Polymer Sci. **32**, 698 (2007)
4. W. Senaratne, L. Andruzzi, C.K. Ober, Biomacromolecules **6**, 2427 (2005)
5. E.P.K. Currie, J. Van der Gucht, Pure Appl. Chem. **71**, 1227 (1999)
6. W. Bosker, P. Iakovlev, W. Norde, M.C. Stuart, J. Coll. Interf. Sci. **286**, 496 (2005)
7. W. Norde, D. Gage, Langmuir **20**, 4162 (2004)
8. A. Halperin, G. Fragneto, A. Schollier, M. Sferrazza, Langmuir **23**, 10603 (2007)
9. A. Halperin, M. Kroger, Langmuir **25**, 11621 (2009)
10. A. Halperin, Langmuir **15**, 2525 (1999)
11. C. Xue, N. Yonet-Tanyeri, N. Brouette, M. Sferrazza, P.V. Braun, D.E. Leckband, Langmuir **27**, 8810 (2011)
12. K.N. Plunkett, X. Zhu, J.S. Moore, D.E. Leckband, Langmuir **22**, 4259 (2006)
13. K. Fukumori, Y. Akiyama, Y. Kumashiro, J. Kobayashi, M. Yamato, K. Sakai, T. Okano, Macromolecular Biosci. **10**, 1117 (2010)
14. Y. Akiyama, A. Kikuchi, M. Yamato, T. Okano, Langmuir **20**, 5506 (2004)
15. K. Fukumori, Y. Akiyama, M. Yamato, J. Kobayashi, K. Sakai, T. Okano, Acta Biomaterialia **5**, 470 (2009)
16. H.E. Canavan, D.J. Graham, X. Cheng, B.D. Ratner, D.G. Castner, Langmuir **23**, 50 (2007)
17. K. Matyjaszewski, P.J. Miller, N. Shukla, B. Immaraporn, A. Gelman, B.B. Luokala, T.M. Siclovan, G. Kickelbick, T. Vallant, H. Hoffmann, T. Pakula, Macromolecules **32**, 8716 (1999)

18. L. Stryer, *Biochemistry* (W. H. Freeman, San Francisco, 1981)
19. R.R. Burgess, *Protein Purification* (Weinheim: WILEY-VCH Verlag GmbH, 2008)
20. A. Papra, N. Gadegaard, N.B. Larsen, Langmuir **17**, 1457 (2001)
21. S. Sharma, R.W. Johnson, T.A. Desai, Langmuir **20**, 348 (2004)
22. R. Cubitt, G. Fragneto, Appl. Phys. A **74**, s329 (2002)
23. K. Yu, H. Wang, L. Xue, Y. Han, Langmuir **23**, 1443 (2007)
24. J.R. Lu, T.J. Su, P.N. Thirtle, R.K. Thomas, A.R. Rennie, R. Cubitt, J. Coll. Interf. Sci. **206**, 212 (1998)
25. G. Fragneto, R. Thomas, A. Rennie, J. Penfold, Science **267**, 657 (1995)
26. D.C. McDermott, J.R. Lu, E.M. Lee, R.K. Thomas, A.R. Rennie, Langmuir **8**, 1204 (1992)
27. G. Fragneto, J.R. Lu, D.C. McDermott, R.K. Thomas, A.R. Rennie, P.D. Gallagher, S.K. Satija, Langmuir **12**, 477 (1996)
28. J. Brandrup, E.H. Immergut, E.A. Grulke, *Polymer Handbook* (4th Edition) (J. W. & Sons, 1999)
29. D. Sunday, S. Curras-Medina, D.L. Green, Macromolecules **43**, 4871 (2010)
30. H. Tu, C.E. Heitzman, P.V. Braun, Langmuir **20**, 8313 (2004)
31. M.O.T. Yang, J. Yamato, Mater. Res. Soc. Bull. **30**, 189 (2005)
32. J. Israelachvili, *Intermolecular and Surface Forces* (Academic Press, New York, 1992)
33. K. Watanabe, M. Yamato, Y. Hayashida, J. Yang, A. Kikuchi, T. Okano, Y. Tano, K. Nishida, Biomaterials **28**, 745 (2007)
34. I.Y. Galaev, B. Mattiasson, Trends Biotechnol. **17**, 335 (1999)
35. N. Idota, A. Kikuchi, J. Kobayashi, Y. Akiyama, K. Sakai, T. Okano, Langmuir **22**, 425 (2006)
36. A. Mizutani, K. Nagase, A. Kikuchi, H. Kanazawa, Y. Akiyama, J. Kobayashi, M. Annaka, T. Okano, J. Chromatogr. B **878**, 2191 (2010)
37. H. Yim, M.S. Kent, S. Satija, S. Mendez, S.S. Balamurugan, S. Balamurugan, G.P. Lopez, Phys. Rev. E **72**, 051801 (2005)
38. A. Halperin, Eur. Phys. J. B **3**, 359 (1998)
39. V.A. Baulin, A. Halperin, Macromol. Theory Simul. **12**, 549 (2003)
40. V.A. Baulin, E.B. Zhulina, A. Halperin, J. Chem. Phys. **119**, 10977 (2003)
41. X. Zhu, C. Yan, F.M. Winnik, D. Leckband, Langmuir **23**, 162 (2007)
42. F. Cecchet, B. De Meersman, S. Demoustier-Champagne, B. Nysten, A.M. Jonas, Langmuir **22**, 1173 (2006)
43. A. Halperin, M. Kroger, Macromolecules **44**, 6986 (2011)